



Assessing the suitability of global evapotranspiration products over irrigated areas

Pierre Laluet¹, Chiara Corbari², Oscar Baez-Villanueva³, Sophia Walther⁴, Yongqiang Zhang⁵, Joaquín Muñoz-Sabater⁶, Gabriel B. Senay⁷, Clément Albergel⁸, and Wouter Dorigo¹

Correspondence: Pierre Laluet (pierre.laluet@geo.tuwien.ac.at)

Abstract. Reliable estimation of evapotranspiration (ET) over irrigated croplands is crucial for agricultural water management, hydrological modeling, and monitoring of land–atmosphere exchanges. Yet the reliability of global ET datasets in these environments remains insufficiently assessed. Here, we evaluate six widely used global ET products (FLUXCOM RS, GLEAM v4.2a, PMLv2, ERA5-Land, MOD16A2, and SSEBop v6.1), covering a wide range of modeling approaches, to assess their ability to capture irrigation-related ET signals. The assessment combines spatial and seasonal evaluations across diverse agroclimatic regions, using three complementary references: a map of area equipped for irrigation, the OpenET ensemble, and eddy covariance measurements from irrigated croplands. Results reveal strong contrasts in how well the products reproduce reference patterns. PMLv2, SSEBop v6.1, and FLUXCOM RS show the highest agreement, effectively capturing irrigation-related spatial and seasonal ET variations. MOD16A2 shows moderate agreement, with consistently lower ET values than the reference datasets. ERA5-Land and GLEAM v4.2a exhibit the weakest correspondence, reflecting limitations linked to their precipitation-driven water-balance soil moisture and stress formulations. Differences among products mainly reflect how water stress is represented and whether irrigation-sensitive variables such as land surface temperature and vegetation properties are incorporated. This multi-scale evaluation provides guidance for selecting ET products in irrigated regions and highlights priorities for improving the representation of irrigation in global ET models.

¹Department of Geodesy and Geoinformation, TU Wien, Vienna, Austria

²Department of Civil and Environmental Engineering, Politecnico di Milano, Milan, Italy

³Hydro-Climate Extremes Lab (H-CEL), Ghent University, Ghent, Belgium

⁴Max Planck Institute for Biogeochemistry, Jena, Germany

⁵Key Laboratory of Water Cycle and Related Land Surface Processes, Institute of Geographic Sciences and Natural Resources Research, Chinese Academy of Sciences, Beijing, China.

⁶European Centre for Medium-Range Weather Forecasts (ECMWF), Reading, UK

⁷USGS Earth Resources Observation and Science Center, North Central Climate Adaptation Science Center, Fort Collins, USA

⁸European Space Agency Climate Office, ECSAT, Didcot, UK





1 Introduction

Evapotranspiration (ET), defined here as the sum of transpiration, soil evaporation, and interception loss, is the largest flux of water returning from land to the atmosphere, accounting for more than 60% of global terrestrial precipitation on average (Oki and Kanae, 2006; Dorigo et al., 2021). Beyond its hydrological role, ET also regulates key energy and carbon exchanges between the land surface and the atmosphere, linking the water, energy, and carbon cycles (Seneviratne et al., 2010; Fisher et al., 2017). In irrigated regions, accurately quantifying ET is particularly important. Although they cover only about 2.5% of the global land surface, irrigation hotspots are key regional drivers of environmental change (McDermid et al., 2023). Irrigation enhances latent heat fluxes, reduces sensible heat fluxes, and contributes to mitigating extreme heat events (Thiery et al., 2017, 2020; Asmus et al., 2023). It also modifies soil moisture, land surface temperature (LST), albedo, and local atmospheric dynamics, with broader effects on precipitation and climate feedbacks (McDermid et al., 2019; Lunel et al., 2024).

A wide range of global ET products has been developed in recent decades and is now publicly available. They differ substantially in methodology and input data. Some rely on machine learning, such as FLUXCOM (Jung et al., 2019) and X-BASE (Nelson* and Walther* et al., 2024). Others are semi-mechanistic, remote sensing—driven models combining physical formulations to estimate the main fluxes with empirical or machine learning approaches to parameterize more complex processes, for example, MOD16A2 (Mu et al., 2011), PMLv2 (Zhang et al., 2019), GLEAM4 (Miralles et al., 2025), or ETMonitor (Zheng et al., 2022). Other approaches are based on simplified energy balance formulations, such as SSEBop (Senay, 2018). In addition, several products are derived from land surface models and reanalyses, such as ERA5-Land (Muñoz-Sabater et al., 2021), GLDAS (Rodell et al., 2004), or MERRA-2 (Gelaro et al., 2017). Across these products, the type of input data varies widely, ranging from meteorological reanalyses, to Earth Observation (EO) variables such as vegetation indices, LST, and albedo, to *in situ* measurements used for training or calibration.

Global ET products are used for a wide range of scientific applications. At the global scale, they support climate studies and model evaluations. For instance, Wang et al. (2021) assessed the realism of ET simulations in CMIP6 climate models by benchmarking them against GLEAM v3.3. ET products are also used to study land–atmosphere interactions; for example, Chen and Dirmeyer (2019) analyzed the impacts of irrigation on LST using ET data from MOD16A2, GLEAM v3, and DOLCE (Hobeichi et al., 2018). In hydrological applications, Alfieri et al. (2022) used GLEAM v3.5a to calibrate a hydrological model in the Po Valley, while Liu et al. (2022) combined PMLv2, GLEAM v3.2, and MOD16A2 with GRACE-derived water storage changes to calibrate a global water balance model across large catchments. ET products have also been used in drought research; for example, Hong et al. (2023) used GLEAM v3.6a to investigate the relationships between ET and drought dynamics in southeastern China. Another important application of global ET products is the quantification of irrigation water use. Kragh et al. (2023) estimated irrigation water use in the Indo-Gangetic Plain by comparing ET from FLUXCOM (Remote Sensing version; RS), MOD16A2, PMLv2, and ERA5-Land with ET simulations from a hydrological model run without irrigation. Similarly, Zhang and Long (2021) used SSEBop and other EO-based ET datasets to estimate irrigation water use across the contiguous United States (CONUS), while Zipper et al. (2024) estimated net irrigation in the U.S. Great Plains as the difference between effective precipitation and the OpenET ensemble (Volk et al., 2024)





Assessing the quality of global ET datasets is critical to ensure their reliable use in agricultural, climate, hydrological, and land–atmosphere studies. However, most existing evaluations have focused on large-scale or global assessments. These typically rely on *in situ* flux tower measurements—as in the LandFlux-EVAL project (Mueller et al., 2013) or the GEWEX LandFlux initiative (McCabe et al., 2016)—or on ET inferred as the residual term of the water balance (e.g. Liu et al., 2016; Lehmann et al., 2022). Many intercomparison efforts have also been conducted as part of the development and evaluation of new ET datasets, typically benchmarking them against existing ET products globally, such as in GLEAM4 (Miralles et al., 2025), FLUXCOM (Jung et al., 2019), ETMonitor (Zheng et al., 2022), or PMLv2 (Zhang et al., 2019). Beyond global evaluations, several studies have assessed the performance of ET products at regional scales. For instance, Etchanchu et al. (2025) evaluated 20 ET products using flux tower observations in a semi-arid region of West Africa, whereas Pascolini-Campbell et al. (2020) and Weerasinghe et al. (2020) used GRACE-based estimates to benchmark ET datasets over large watersheds in the

Yet, irrigated croplands remain largely underrepresented in these evaluation efforts. Only a handful of studies have explicitly targeted intensively irrigated regions. For example, McNamara et al. (2021) evaluated multiple ET products in the Nile Basin using GRACE-derived ET estimates and identified PMLv2 and WaPOR (FAO, 2018) as the best-performing datasets. In northern Thailand, Sriwongsitanon et al. (2020) intercompared several products over an irrigated catchment and found that MOD16A2 best reproduced the spatial distribution of irrigation. More recently, Crow et al. (2025) evaluated the sensitivity of a thermal infrared (TIR)-based ET product (ALEXI; Anderson et al. 1997) and microwave soil moisture observations (SMAP; Entekhabi et al. 2010) to irrigation signals across the CONUS. Using the MIrAD-US irrigation map and flux tower measurements as references, they found that ALEXI-based ET captured irrigation-related spatial and seasonal patterns more clearly than SMAP soil moisture.

These studies demonstrate that some global ET datasets capture irrigation signals more effectively than others, yet existing evaluations remain limited in both spatial coverage and methodological scope. Consequently, our understanding of product reliability over irrigated areas remains very limited, and no comprehensive assessment has yet been conducted across diverse geographic and climatic settings while systematically analyzing multiple global ET datasets.

To address this gap, we present a multi-scale, multi-source assessment of six widely used global ET products: FLUXCOM RS, ERA5-Land, SSEBop v6.1, GLEAM v4.2a, PMLv2, and MOD16A2. Our evaluation integrates three complementary assessments conducted at different spatial scales and based on distinct reference datasets. First, we assess the spatial coherence between ET products and irrigation infrastructure maps across seven major irrigated regions in the CONUS, Europe, and South Asia. Second, we evaluate the seasonal dynamics of ET by comparing the products with ensemble estimates from OpenET, which provides an independent multi-model benchmark, over four irrigated areas in the CONUS. Finally, we conduct a local-scale assessment using eddy covariance tower data from two irrigated sites in the Po Valley, Italy.



105



2 Material and methods

2.1 Global ET products

The six selected ET products represent diverse modeling strategies and input data sources, spanning machine learning approaches, energy balance formulations, and reanalysis-driven land surface models. None of these products explicitly simulates irrigation; rather, irrigation effects may be implicitly captured depending on the nature of the input data and, in particular, on how water stress is represented within each model.

FLUXCOM RS (Jung et al., 2019) is based on a machine learning algorithm trained on data from 224 flux towers from the FLUXNET La Thuile synthesis dataset and the CarboAfrica network (Valentini et al., 2014). Among these, 27 sites are croplands, including seven irrigated ones. The model uses MODIS-based predictors—LST, land cover type, fraction of absorbed photosynthetically active radiation (fAPAR), enhanced vegetation index (EVI)—as well as net radiation (Rn) from CERES.

GLEAM v4.2a (Miralles et al., 2025) is a hybrid ET model that combines physically-based processes with machine learning. Rainfall interception is estimated using the global van Dijk–Bruijnzeel model (van Dijk and Bruijnzeel, 2001), constrained by satellite-derived vegetation data and a meta-analyses of field experiments (Zhong et al., 2022). Potential evapotranspiration (PET) is calculated using Penman's equation, explicitly accounting for wind speed, vegetation height, and vapour pressure deficit (VPD). GLEAM v4.2a solves a multi-layer soil water balance that includes plant access to groundwater (Hulsman et al., 2023) and assimilates surface soil moisture from ESA CCI (Dorigo et al., 2017). ET is obtained by constraining PET with an evaporative stress factor estimated via a deep neural network that captures complex environmental interactions using modeled root-zone soil moisture, VOD, VPD, incoming solar radiation, air temperature, CO₂, wind speed, and leaf area index (LAI) data as predictors (Koppa et al., 2022).

MOD16A2 (Mu et al., 2011) is based on a modified version of the Penman–Monteith equation that integrates MODIS-derived surface and vegetation properties (LAI, fAPAR, albedo) with meteorological inputs from the NASA GMAO (GEOS-5) reanalysis, including air temperature and VPD. Water stress is represented through the surface resistance term (r_s) , which combines stomatal regulation based on VPD and minimum air temperature (T_{\min}) with canopy scaling driven by MODIS LAI and fAPAR.

ERA5-Land (Muñoz-Sabater et al., 2021) is a reanalysis product built on the H-TESSEL land surface model. ET is physically modeled using the Penman–Monteith equation, based on net radiation (Rn), soil heat flux, aerodynamic resistance (r_a) , surface resistance (r_s) , and vapor pressure deficit (VPD). Rn is computed from ERA5 radiative fluxes, while the remaining terms are derived from ERA5 atmospheric fields and pre-defined land-surface properties. Although ERA5-Land does not directly assimilate satellite observations, satellite information can still influence the product indirectly through the atmospheric forcing inherited from ERA5. Vegetation water stress is represented through the formulation of r_s , which depends on root-zone soil moisture simulated by the model's soil water balance and on VPD.

SSEBop v6.1 (Senay et al., 2023) is based on a simplified surface energy balance approach. In version 6.1 used here, ET is calculated as the product of a reference evapotranspiration (ET₀)—taken from climatological Penman–Monteith fields provided by TerraClimate (Abatzoglou et al., 2018)—and an evaporative fraction (ETf) derived from VIIRS-based LST (Hulley



120

125

130



et al., 2018). ETf is determined by comparing each pixel's LST to a dynamically estimated "cold/wet" reference temperature representing maximum ET conditions. This reference temperature is computed locally within a 5 × 5 km moving window using NDVI–LST relationships to identify well-watered vegetation, following the FANO algorithm of Senay et al. (2023).

PMLv2 (Zhang et al., 2019) uses a semi-mechanistic model based on a modified Penman–Monteith equation. Vegetation water stress is accounted for via VPD derived from GLDAS-2.1 simulations and regulates both stomatal conductance and surface resistance. The model's VPD response is calibrated separately for each biome using observations from 95 flux towers, including 11 in the *cropland* biome—four of which are irrigated. Model inputs include MODIS-derived variables (LAI, albedo, and emissivity) as well as daily meteorological forcings from GLDAS-2.1, such as precipitation, air temperature, humidity, radiation, and wind speed.

For intercomparison purposes, all ET datasets were resampled to a common 0.1° grid (that of GLEAM v4.2a) to ensure spatial consistency. Products with native resolution finer then 0.1° were aggregated using area-weighted averaging, while ERA5-Land (native 0.1°) was bilinearly interpolated to ensure grid alignment. Monthly means were then computed for all datasets.

Figure 1 illustrates the average ET during the peak irrigation season (July-August) across the CONUS for the period 2012-2020, for each product. Table 1 summarizes the datasets' spatial and temporal resolutions, available periods, and data sources. Note that SSEBop v6.1 covers a shorter period (2012–2025), while the others extend back to 2001 or 2000.

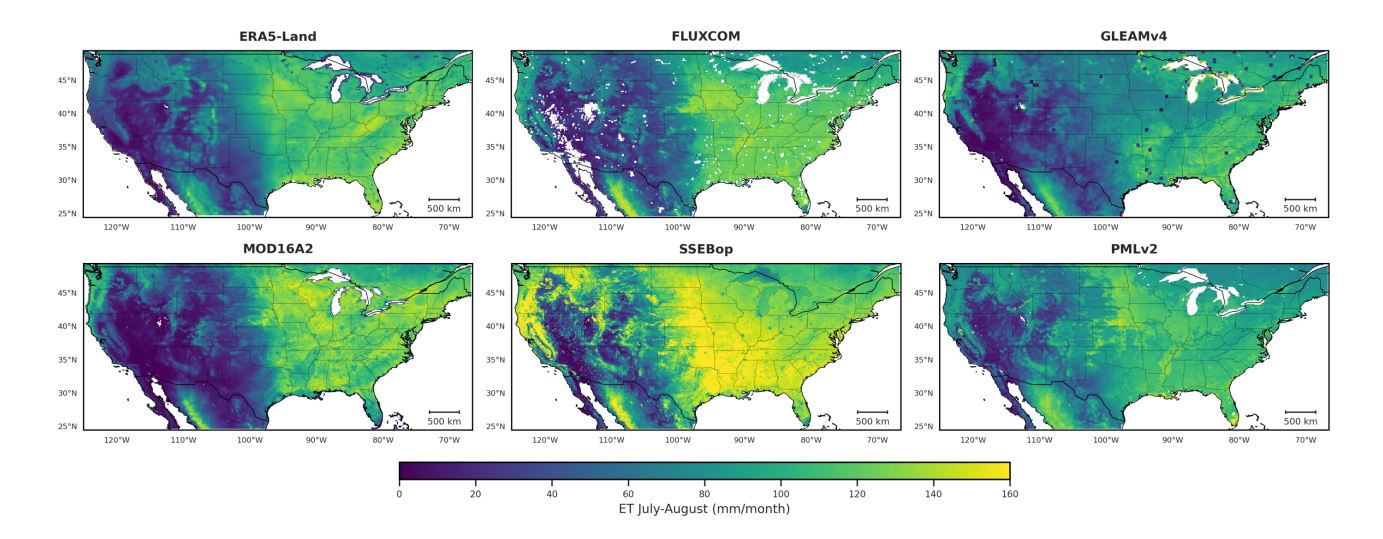


Figure 1. Mean ET (2012-2020) during the peak irrigation season (July–August) over the CONUS for the six ET products, after resampling all datasets onto the common 0.1° GLEAM4 grid.





Table 1. Main characteristics and download sources of the six assessed ET products.

Dataset	Version	Original resolution	Original temporal resolution	Available period	Download source
FLUXCOM	RS	0.0833°	8-day	2001–2020	FLUXCOM portal
GLEAM4	v4.2a	0.1°	Daily	2000-2025	GLEAM website
MOD16A2	v6	500 m	8-day	2001-2023	Google Earth Engine
ERA5-Land	2025 CDS release	0.1°	Hourly	2000-2025	Copernicus CDS
SSEBop	v6.1	1 km	Dekadal	2012-2025	USGS FEWS NET
PMLv2	v0.1.8	500 m	8-day	2000-2023	Google Earth Engine

2.2 Datasets used for evaluation

2.2.1 Map of area equipped for irrigation

The Global Map of Irrigated Areas version 5 (GMIAv5; Siebert et al. 2013), provided at a spatial resolution of 0.0833°, compiles subnational statistical information from administrative units, national census data, and international reports on irrigated areas for the period 2000–2008. In addition, GMIAv5 includes a country-level quality-control flag ranging from "very poor" to "excellent", which reflects the availability, detail, and internal consistency of the underlying national statistics. For instance, the data quality is rated as "very good" for Italy and Spain, and "good" for the United States, India, and Pakistan. We used this map to evaluate whether the ET products can capture the spatial extent of irrigated areas. The underlying assumption is that, within a given grid cell, a higher degree of area equipped for irrigation should correspond to higher ET during the irrigation season. To test this hypothesis, we rescaled the GMIAv5 dataset to match the spatial resolution and grid geometry of the ET products, and computed Pearson's correlation coefficient between the percentage of land equipped for irrigation and the corresponding monthly ET estimates for each product.

2.2.2 OpenET

135

140

The OpenET platform (Melton et al., 2022) represents a consensus effort to operationalize multiple well-established ET models under a common framework, combining six models to estimate ET. Four of these are based on surface energy balance
approaches: METRIC (Allen et al., 2007), DisALEXI (Anderson et al., 2007), geeSEBAL (Bastiaanssen et al., 1998), and
SSEBop (Senay et al., 2013). In addition, the platform includes PT-JPL (Fisher et al., 2008), a simplified formulation of the
Penman–Monteith equation, and SIMS (Melton et al., 2012), an agro-hydrological model that incorporates crop-specific phenology and irrigation schedules. All six models rely on Landsat 30 m imagery, using LST and vegetation parameters derived
from optical and thermal bands.

Among the OpenET models, SSEBop is also included in the set of global ET products evaluated in this study. However, the version assessed here (v6.1) differs from the one used in OpenET in two key aspects: (1) v6.1 derives LST from VIIRS rather than Landsat, and (2) v6.1 computes reference evapotranspiration (ET $_0$) using meteorological inputs from TerraClimate, whereas OpenET uses gridMET.



170



OpenET was selected as a benchmark for the CONUS because it provides a unique ensemble of independently developed models, widely used in operational water management and irrigation monitoring (Allen et al., 2007; Senay et al., 2016; Knipper et al., 2019; Volk et al., 2024). While not a direct ground truth, OpenET offers a spatially explicit reference constrained by satellite data for assessing the relative consistency of global ET products in irrigated regions. Accordingly, it is used here not as an absolute validation dataset, but as an additional benchmark to evaluate the agreement in spatial and seasonal ET dynamics across independent modeling approaches. In this study, we use the OpenET ensemble product, defined as the median of the six model estimates.

2.2.3 Eddy covariance measurements

To evaluate the performance of the selected datasets against *in situ* measurements, we used data from two eddy-covariance towers located in irrigated croplands of the Po Valley, northern Italy: Landriano (45.31°N, 9.27°E) and Livraga (45.18°N, 9.57°E) as observed in Figure 2.

Both towers are installed in irrigated maize fields. The Landriano site provides data for 2008–2011 (Masseroni et al., 2013), and Livraga for 2011–2014 (Nana et al., 2014). Data processing followed standard community protocols, including Webb–Pearman–Leuning (WPL) corrections, filtering of non-stationary periods, and coordinate rotation. Missing values were linearly interpolated, and the resulting time series were aggregated to monthly means to match the temporal resolution of the global ET products.

A key challenge when using eddy covariance tower data for product evaluation lies in the spatial scale mismatch: tower footprints typically range from 100 to 300 m, whereas the ET products analyzed here have a resolution of approximately 10 km. To mitigate this discrepancy, we ensured that both towers are located within homogeneous agricultural landscapes dominated by irrigated maize. Figure 2 shows the 0.1° grid cells (in red) from the analyzed ET datasets, overlaid with irrigated maize plots (in green) as identified by the 2021 WorldCereal database (Van Tricht et al., 2023). The grid cell containing the Livraga site includes 46% irrigated maize, while the one containing the Landriano site includes 34%. The remaining areas are mostly classified as temporary crops (e.g., soybean, rice, or other annuals), which are not labeled as irrigated in the WorldCereal dataset, although both soybean and rice are in practice often irrigated in the Po Valley. These two sites were not involved in the training or calibration of any of the evaluated ET products.





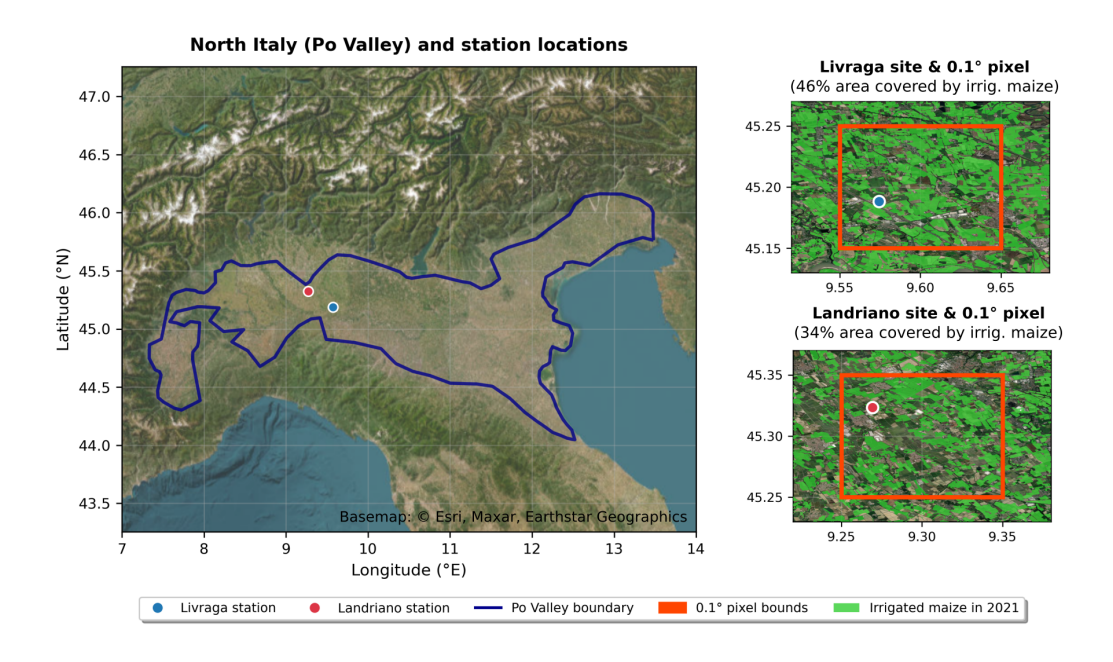


Figure 2. Left: location of the two irrigated maize flux sites (Landriano and Livraga) in the Po Valley, northern Italy. Right: Contour of the 0.1° pixels from the ET datasets (in red), including the tower locations; green areas show irrigated maize plots from the 2021 WorldCereal database.

180 2.3 Study areas

We selected seven intensively irrigated regions distributed across the CONUS, Europe, and South Asia as showcased in Figure 3. The figure also shows the percentage of land area equipped for irrigation, as reported by GMIAv5 (Siebert et al., 2013).

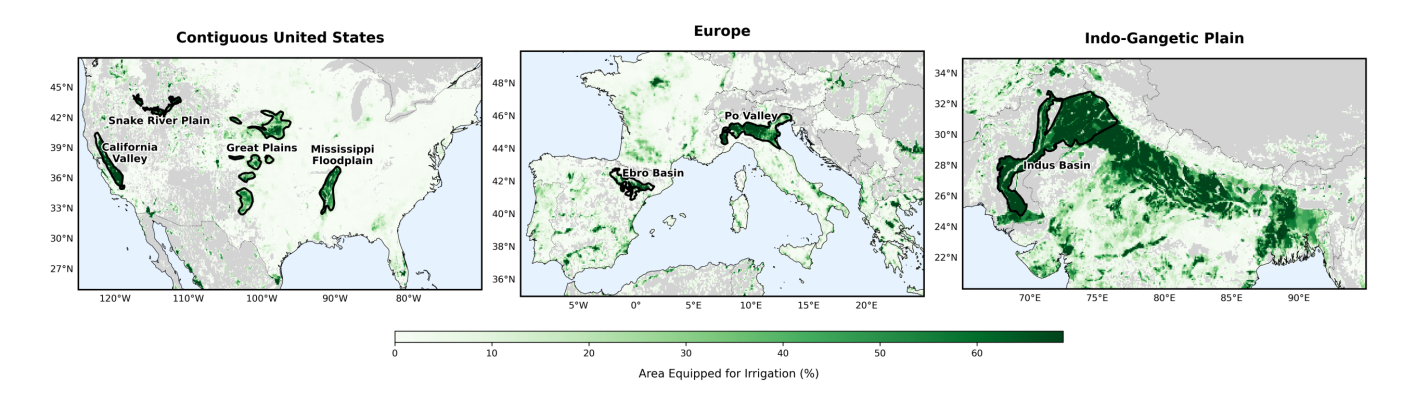


Figure 3. Locations of the seven irrigated regions analyzed in this study, with percentage of area equipped for irrigation from GMIAv5 (Siebert et al., 2013).





Table 2 summarizes the main characteristics of the selected regions, including total area, timing of the peak irrigation season, and average monthly precipitation (from MSWE v2.8; Beck et al. 2019), potential evapotranspiration (PET) from GLEAM v4.2a, and aridity index (P/PET), all computed over the peak irrigation season. The table also reports the average percentage of land equipped for irrigation and specifies the type of evaluation conducted in each region: spatial correspondence with irrigated area (irrig. area), comparison with the OpenET ensemble (OpenET), or performance evaluation against *in situ* eddy covariance data (flux towers).

Table 2. Main characteristics of the seven irrigated regions, including climate indicators and specific assessment conducted in each region.

Region	Area (km²)	Peak season	PET peak season (mm/month)	P peak season (mm/month)	Aridity index peak season (-)	Mean area equipped for irrig. (%)	Analysis
Ebro Basin	19,414	Jun-Aug	160.0	29.0	0.18	30.4	irrig. area
California Valley	48,636	Jul-Aug	188.2	0.9	0.00	60.2	irrig. area, OpenET
Great Plains	139,028	Jul-Aug	190.7	64.6	0.34	34.9	irrig. area, OpenET
Mississippi Flood.	59,117	Jul-Aug	166.0	87.0	0.52	48.6	irrig. area, OpenET
Snake River Plain	21,396	Jul-Aug	158.1	11.8	0.07	50.2	irrig. area, OpenET
Indus Basin	215,491	Jan-Dec	113.0	29.5	0.26	74.0	irrig. area
Po Valley	39,468	Jun-Aug	130.7	65.3	0.50	50.8	irrig. area, flux towers

2.4 Evaluation metrics

We quantified the agreement between ET products and the reference datasets using three standard metrics: Pearson's correlation coefficient (*R*), root mean square deviation (RMSD), and mean bias (defined as ET_{product} – ET_{reference}). For the comparison against eddy-covariance measurements and OpenET, all metrics were computed over the growing-season months only. For the evaluation against the map of areas equipped for irrigation, we assessed spatial consistency by computing pixel-wise correlations between ET and the corresponding fractions of irrigated areas.

195 3 Results

3.1 Comparison with area equipped for irrigation: spatial evaluation

Figure 4 and Table 3 summarize the relationship between mean ET during the peak irrigation season (as defined in Table 2) and the percentage of area equipped for irrigation. Figure 4 presents pixel-wise scatterplots for each product and study region, showing how mean monthly ET varies with the proportion of irrigated area within each grid cell. Table 3 reports the corresponding Pearson correlation coefficients, with an additional row summarizing the average performance of each dataset across all regions.





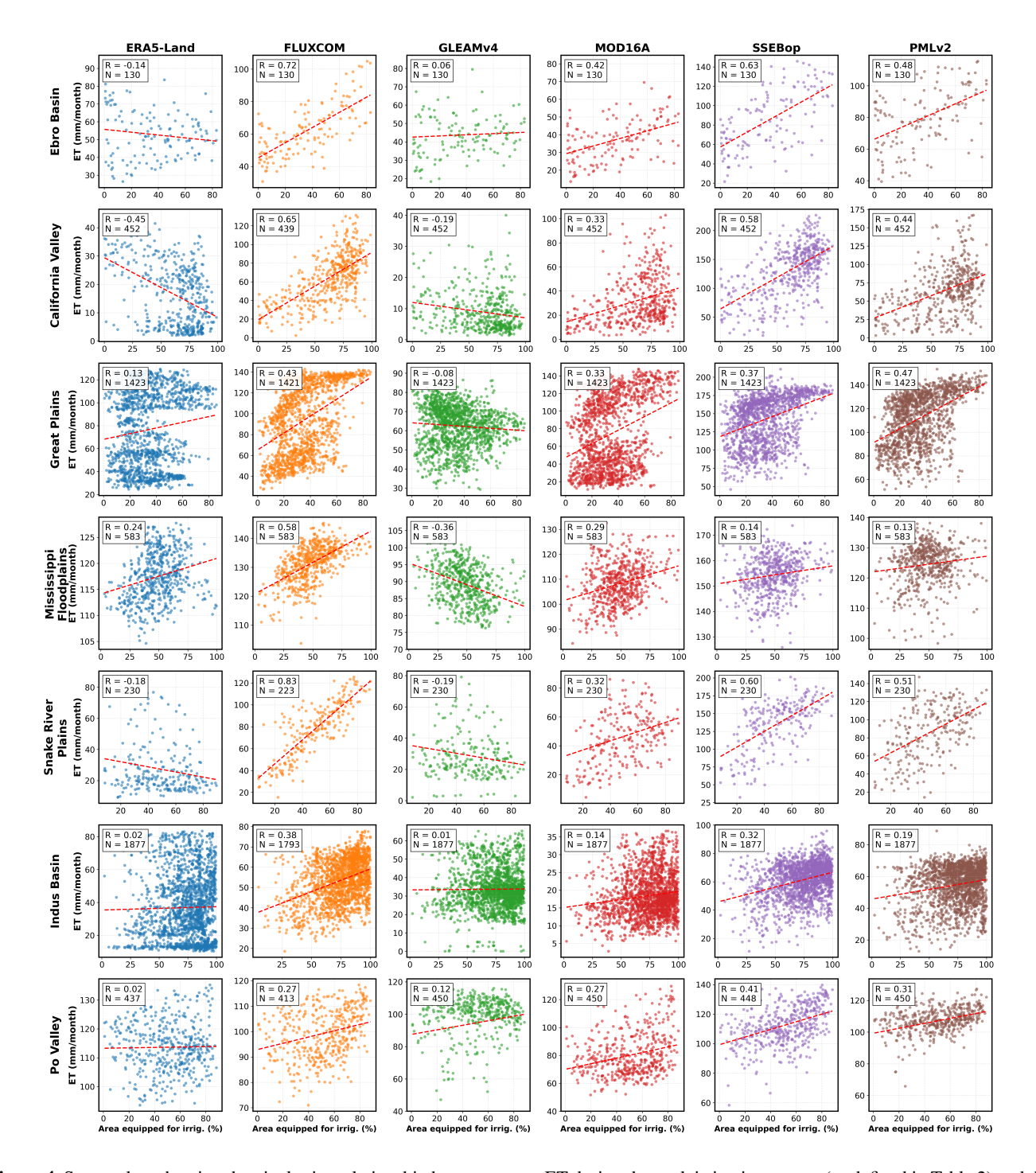


Figure 4. Scatterplots showing the pixel-wise relationship between mean ET during the peak irrigation season (as defined in Table 2) and the fraction of area equipped for irrigation, for each ET product and irrigated region. N denotes the number of valid grid cells included in each correlation analysis.



205

210



Table 3. Pearson correlation coefficients between mean ET during the peak irrigation season and the percentage of land equipped for irrigation for each ET product and irrigated region. Values ≥ 0.30 are highlighted in bold.

Region	ERA5-Land	FLUXCOM RS	GLEAMv4.2a	MOD16A2	SSEBop v6.1	PMLv2
California Valley	-0.45	0.65	-0.19	0.33	0.58	0.44
Great Plains	0.13	0.43	-0.08	0.33	0.37	0.47
Mississippi Floodplain	0.24	0.58	-0.36	0.29	0.14	0.13
Snake River Plain	-0.18	0.83	-0.18	0.32	0.60	0.51
Ebro Basin	-0.14	0.72	0.06	0.42	0.63	0.48
Po Valley	0.02	0.27	0.12	0.27	0.41	0.31
Indus Basin	0.02	0.38	0.01	0.14	0.32	0.19
Mean across datasets	-0.05	0.55	-0.09	0.30	0.44	0.36

The results highlight substantial differences in the ability of the six ET products to reproduce irrigation-related spatial patterns. FLUXCOM RS shows the strongest overall correspondence with the fraction of land equipped for irrigation (mean R=0.55), followed by SSEBop v6.1 (R=0.44), PMLv2 (R=0.36), and MOD16A2 (R=0.30). In contrast, ERA5-Land (R=-0.05) and GLEAMv4.2a (R=-0.09) exhibit no clear spatial correlation with the area equipped for irrigation. This relative ranking is consistent across four of the seven study regions: the California Central Valley, Snake River Plain, Ebro Basin, and Indus Basin.

Strong regional contrasts are also evident. Excluding ERA5-Land and GLEAM v4.2a, correlations averaged across the remaining products are highest in the Snake River Plain (R=0.57), Ebro Basin (R=0.56), and California Valley (R=0.50), while lower R values are found in the Mississippi Floodplain (R=0.29) and Indus Basin (R=0.26). FLUXCOM RS, SSEBop v6.1, PMLv2, and MOD16A2 better capture irrigation-related ET patterns in arid to semi-arid regions such as the Ebro Basin, California Central Valley, and Snake River Plain (aridity index < 0.3), where irrigation produces sharper ET contrasts with non-irrigated areas. A notable exception is the Indus Basin, which, despite its arid climate and extensive irrigation, exhibits relatively weak correlations for both PMLv2 and MOD16A2.

215 3.2 Comparison with OpenET: seasonal dynamics and magnitude assessment

Figure 5 shows the time series of the six ET products (colored lines) compared with the OpenET ensemble (black line) from 2016 to 2023 across four major irrigated regions in the CONUS: the California Valley, Snake River Plain, Mississippi Floodplain, and Great Plains. The corresponding seasonal cycles are also displayed. Table 4 reports statistical metrics describing the agreement between the ET products and OpenET during the main irrigation season (April–September). Metrics include the Pearson correlation coefficient (*R*), RMSD, mean bias, and average ET, all computed over April–September.





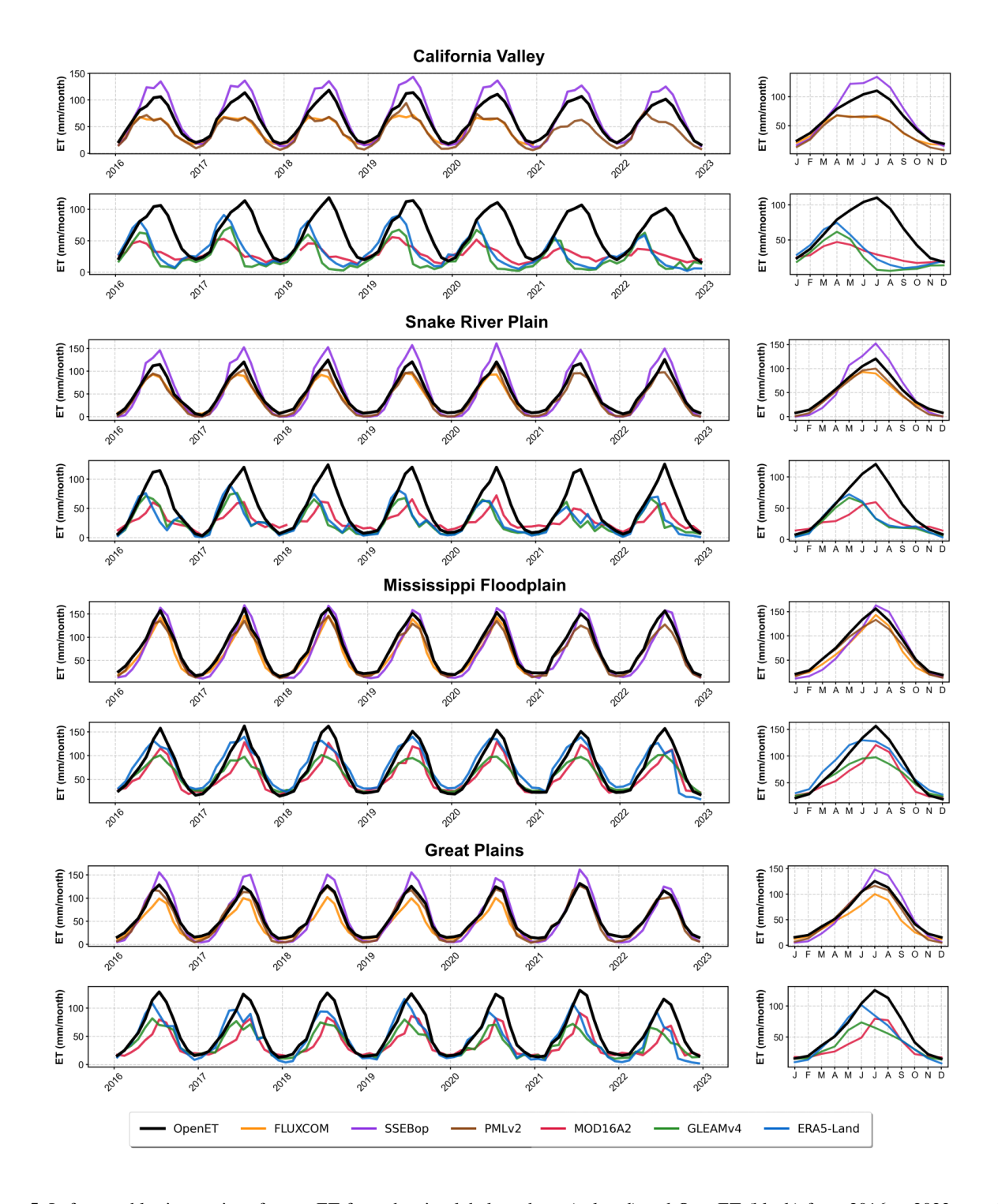


Figure 5. Left: monthly time series of mean ET from the six global products (colored) and OpenET (black) from 2016 to 2023 over four major irrigated regions in the CONUS. Right: the corresponding seasonal cycles.





225

230

Table 4. Statistical comparison between ET products and OpenET across four irrigated regions in the CONUS during the main irrigation season (April–September). Metrics include the Pearson correlation coefficient (*R*), RMSD, mean bias, and mean ET. For OpenET, the mean seasonal ET is reported.

Region	Product	R [-]	RMSD [mm/month]	Mean bias [mm/month]	Mean [mm/month]
	FLUXCOM RS	0.68	34.8	-32.9	59.6
	SSEBop v6.1	0.94	20.7	18.9	109.9
	PMLv2	0.58	34.0	-31.4	59.7
California Valley	MOD16A2	0.13	60.4	-57.8	33.3
Ž	GLEAMv4.2a	-0.15	71.5	-64.5	26.6
	ERA5-Land	0.02	63.2	-54.8	36.2
	OpenET	-	_	_	91.0
	FLUXCOM RS	0.92	17.7	-14.8	70.7
	SSEBop v6.1	0.95	23.7	18.3	103.3
	PMLv2	0.95	14.1	-11.7	73.3
Snake River Plain	MOD16A2	0.91	46.3	-44.5	40.5
	GLEAMv4.2a	0.08	53.4	-43.8	41.2
	ERA5-Land	0.04	51.9	-40.6	44.4
	OpenET	-	_	_	85.0
	FLUXCOM RS	0.97	18.6	-17.2	98.4
	SSEBop v6.1	0.91	17.0	-4.1	111.7
	PMLv2	0.97	15.6	-13.1	102.7
Mississippi Floodplain	MOD16A2	0.92	33.1	-31.3	84.4
	GLEAMv4.2a	0.92	36.8	-32.4	83.3
	ERA5-Land	0.66	21.8	-5.1	110.6
	OpenET	-		-	115.7
	FLUXCOM RS	0.93	23.6	-21.4	70.5
	SSEBop v6.1	0.96	16.9	10.5	101.5
	PMLv2	0.97	7.2	-2.4	88.6
Great Plains	MOD16A2	0.92	40.0	-38.5	52.5
	GLEAMv4.2a	0.64	40.5	-35.2	55.9
	ERA5-Land	0.52	30.6	-18.8	72.2
	OpenET	_	_	_	91.0

Clear differences emerge in the magnitude and seasonal variability of ET across products. SSEBop v6.1 stands out with the highest average ET during the irrigation season (106.6 mm/month), closely aligning with the magnitude and temporal dynamics of OpenET, with a mean bias of +10.9 mm/month and a very high correlation (R=0.94). In contrast, MOD16A2 yields the lowest mean ET (52.7 mm/month), showing substantially lower values than OpenET during the irrigation season (mean bias of -43.0 mm/month) and a weaker correspondence in temporal variability (R=0.72). Overall, most products estimate lower ET than OpenET, with the largest negative mean bias observed for MOD16A2, ERA5-Land, and GLEAM v4.2a.

Across regions, FLUXCOM RS, PMLv2, SSEBop v6.1, and MOD16A2 show the strongest correspondence with the benchmark, with a global mean correlation of R=0.89 when averaged across datasets and regions. However, this agreement is not spatially uniform: in the California Valley, for instance, only SSEBop v6.1 exceeds R=0.7, whereas FLUXCOM RS and PMLv2 show higher correlations in the Snake River Plain and Great Plains. FLUXCOM RS and PMLv2 also display a close mutual consistency in both magnitude and seasonality, yielding the lowest mean RMSDs across regions (23.6 and 7.2 mm/month, respectively).



235

240



ERA5-Land and GLEAM v4.2a exhibit weaker agreement with the ensemble benchmark, particularly in drier regions such as the California Valley, Snake River Plain, and Great Plains, while their correspondence improves in the more humid Mississippi Floodplain. Their mean RMSDs across regions remain relatively high (41.9 mm/month for ERA5-Land and 50.6 mm/month for GLEAM v4.2a).

Beyond these statistical metrics, differences also emerge in the timing of seasonal peaks. OpenET and SSEBop v6.1 show a consistent maximum in July, reflecting irrigation demand, and this seasonal pattern is generally reproduced by MOD16A2, FLUXCOM RS, and PMLv2. In the California Valley, however, the July peak is weaker in FLUXCOM RS and PMLv2, and largely absent in MOD16A2. In contrast, GLEAM v4.2a and ERA5-Land tend to peak earlier, typically in spring, although both show a modest secondary maximum in July over the more humid Mississippi Floodplain.

3.3 Comparison with eddy-covariance data: seasonal dynamics and magnitude assessment

Figure 6 shows the time series of the six ET products (colored lines) compared with flux tower measurements (black line) at two irrigated maize sites in the Po Valley: Livraga (top) and Landriano (bottom). The corresponding seasonal cycles are also shown. Table 5 summarizes the agreement of each dataset with the tower measurements during the April–September irrigation season. Metrics include the Pearson correlation coefficient (R), RMSD, mean bias, and mean ET, all calculated over the irrigated season (April–September). The table also reports the number of months included in the metrics computation. Reported R values are accompanied by two-tailed significance levels (p < 0.05 (*), p < 0.01 (***), p < 0.001 (***), n = 1.000 significant).

FLUXCOM RS, PMLv2, and MOD16A2 show strong temporal agreement with the flux tower data at both sites, with mean correlation coefficients of 0.88, 0.90, and 0.91, respectively. SSEBop v6.1 also shows a high correlation (R = 0.93) during the nine-month period when data overlap at Livraga. Notably, FLUXCOM RS and PMLv2 exhibit very similar seasonal dynamics and mean ET magnitudes. In contrast, GLEAM v4.2a and ERA5-Land show weaker correspondence, with average correlations of 0.77 and 0.71, respectively.

Regarding magnitude differences, PMLv2 and SSEBop v6.1 display the lowest mean RMSD values (24.3 and 23.3 mm month⁻¹ on average, respectively), followed by ERA5-Land (28.4), FLUXCOM RS (29.1), GLEAM v4.2a (30.1), and MOD16A2 (40.4 mm month⁻¹). All products tend to underestimate ET relative to tower measurements, with MOD16A2 showing the strongest negative bias (-34.2 mm month⁻¹ on average).





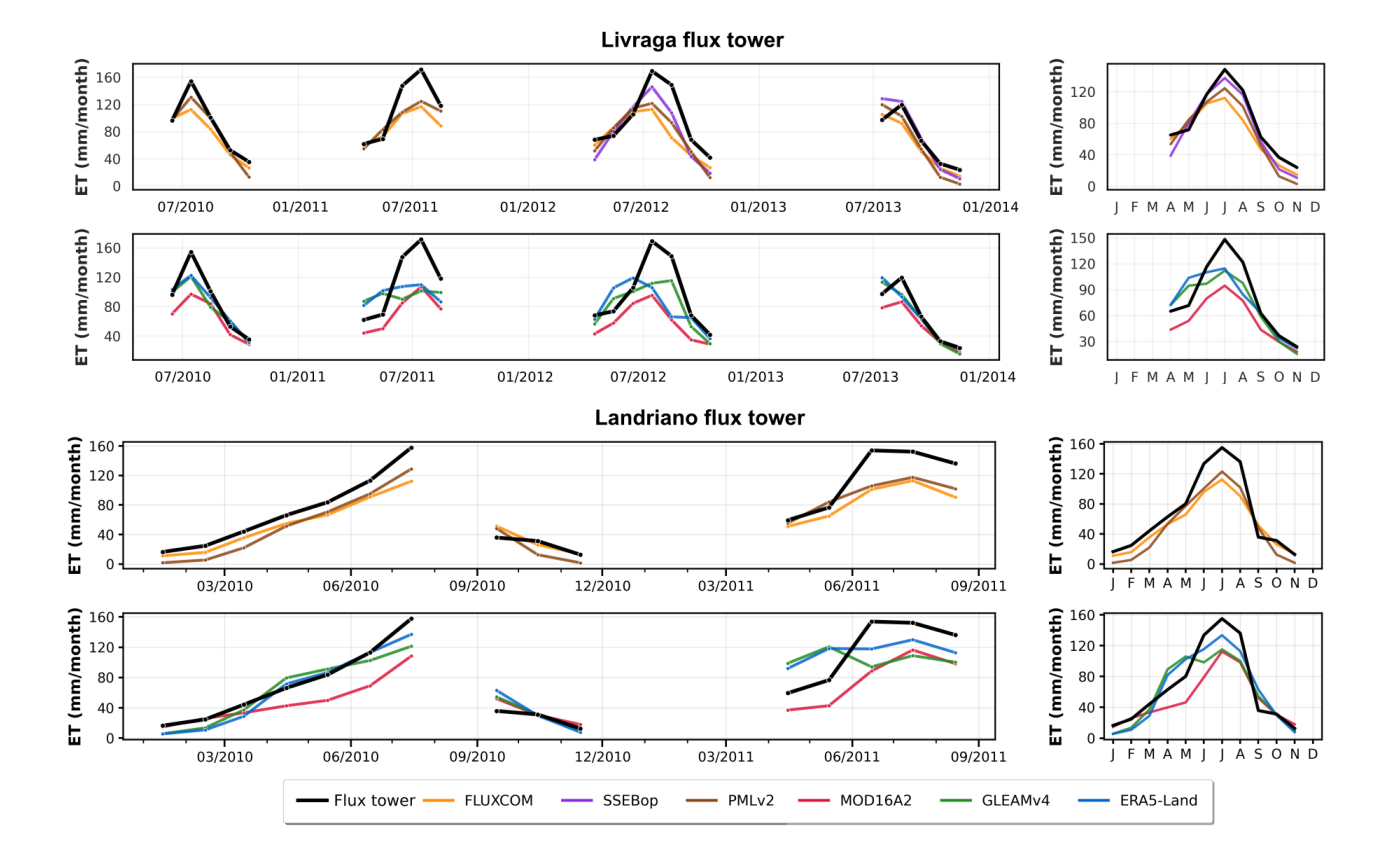


Figure 6. Left: monthly ET time series from the six global products (colored) and eddy-covariance measurements (black) at the Livraga (top) and Landriano (bottom) sites. Right: the corresponding seasonal cycles.

Table 5. Comparison of the six ET products with eddy-covariance measurements at the Livraga and Landriano sites during the main irrigation season (April–September). Metrics include the Pearson correlation coefficient (R), RMSD, mean bias, and mean ET, along with the number of months (N) and correlation significance levels (*p < 0.05, **p < 0.01, ***p < 0.001; ns = not significant).

Site	Product	R [-]	RMSD [mm/month]	Bias [mm/month]	Mean ET (in situ)	Mean ET (product)	N [months]	p-value	Signif.
	ERA5-Land	0.51	35.2	-12.4	105.0	92.6	18	0.0316	*
	FLUXCOM RS	0.78	32.2	-20.6	105.0	84.4	18	0.0001	***
	GLEAMv4.2a	0.71	31.2	-14.0	105.0	91.0	18	0.0011	**
Livraga	MOD16A2	0.86	42.1	-35.4	105.0	69.6	18	< 0.0001	***
	PMLv2	0.83	25.4	-13.1	105.0	91.9	18	< 0.0001	***
	SSEBop v6.1	0.81	23.3	-6.8	101.9	95.0	9	0.0083	**
	ERA5-Land	0.86	25.2	0.7	103.5	104.2	10	0.0013	**
	FLUXCOM RS	0.97	31.4	-23.8	103.5	79.6	10	< 0.0001	***
	GLEAMv4.2a	0.61	35.0	-6.4	103.5	97.1	10	0.0609	ns
Landriano	MOD16A2	0.91	38.7	-33.0	103.5	70.5	10	0.0002	***
	PMLv2	0.96	25.4	-17.6	103.5	85.9	10	< 0.0001	***
	SSEBop v6.1	-	_	- 1 <i>E</i>	_	_	-	_	_



270



3.4 Interannual variability of ET products and sensitivity to drought

Figure 7 shows time series of monthly ET anomalies during the irrigation season (April–September) in the California Valley for the six ET datasets (first six rows), along with NDVI anomalies from MODIS (last row). Anomalies were computed over the common period 2001–2020, except for SSEBop v6.1, for which they were calculated over the period 2012–2020. The 5th (P5) and 95th (P95) percentiles were computed over the 2012–2020 period. The yellow-shaded area highlights the 2014 irrigation season, during which severe water restrictions were implemented across the California Valley (California Department of Water Resources, 2021). Table 6 summarizes the P5 and P95 values, along with the corresponding z-scores for June and July 2014, indicating the number of standard deviations from the 2012–2020 mean.

The amplitude of interannual ET anomalies varies substantially across datasets. GLEAM v4.2a and ERA5-Land exhibit the largest variability, with P5 values of -14.8 and -25.4 mm month⁻¹ and P95 values of 16.9 and 17.9 mm month⁻¹, respectively. In contrast, FLUXCOM RS displays much lower variability (P5 = -5.3, P95 = 2.3 mm month⁻¹), while SSEBop v6.1, PMLv2, and MOD16A2 fall within an intermediate range. Notably, in 2017, PMLv2 and MOD16A2 indicate pronounced negative ET anomalies despite NDVI anomalies being positive in spring and only slightly negative in summer, whereas FLUXCOM RS and the other datasets mainly capture positive ET anomalies during this period.

During the 2014 irrigation season, when water use was heavily restricted, all datasets captured marked negative ET anomalies. Relative to their own historical variability, FLUXCOM RS shows the strongest response, with z-scores of –2.29 (June) and –1.96 (July), indicating anomalies near or below the 2.5th percentile of their historical distribution. PMLv2 (–1.24, –1.78), ERA5-Land (–1.34, –1.45), and SSEBop v6.1 (–1.49, –1.63) also reflect substantial negative anomalies. MOD16A2 and GLEAM v4.2a exhibit lower z-scores (around –1), suggesting that 2014 appears less exceptional in the context of their own anomaly distributions.





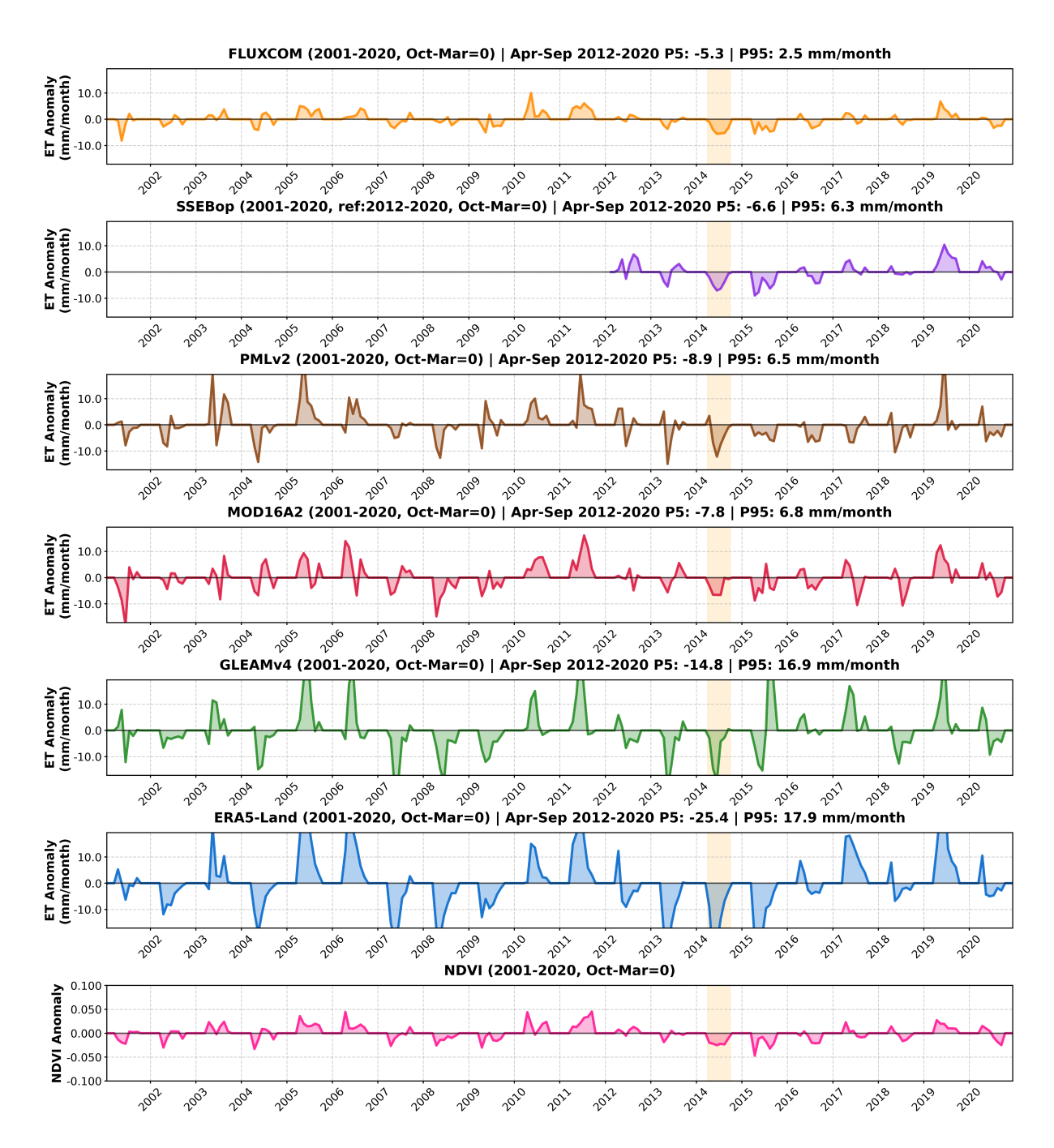


Figure 7. Monthly anomalies during the irrigation season (April–September) in the California Valley for the six ET datasets (first six rows) and MODIS NDVI (last row). The shaded area indicates the 2014 irrigation restrictions.





Table 6. ET anomalies and corresponding z-scores (computed over 2012–2020) for June and July 2014 in the California Valley during the irrigation restrictions.

Dataset	June 2014 Anomaly (mm/month)	June 2014 Z-score (-)	July 2014 Anomaly (mm/month)	July 2014 Z-score
FLUXCOM RS	-5.6	-2.29	-5.4	-1.96
SSEBop v6.1	-7.0	-1.49	-6.4	-1.63
PMLv2	-12.1	-1.24	-7.5	-1.78
MOD16A2	-6.6	-1.06	-6.6	-0.96
GLEAM v4.2a	-19.2	-1.06	-4.3	-0.84
ERA5-Land	-23.7	-1.34	-13.7	-1.45

4 Discussion

285

290

295

300

Based on the assessment results, FLUXCOM RS, PMLv2, and SSEBop v6.1 show the highest overall consistency with reference datasets over irrigated areas. Although a strict ranking is difficult to establish, FLUXCOM RS exhibits the strongest spatial correspondence with irrigated areas, whereas PMLv2 shows better agreement than the other datasets with both OpenET and flux tower data in terms of seasonal dynamics and magnitude. Notably, FLUXCOM RS and PMLv2 display very similar ET patterns, and both tend to produce slightly lower ET values, while SSEBop v6.1 generally yields higher estimates.

MOD16A2 exhibits intermediate consistency, capturing some spatial and temporal irrigation signals, but generally yields lower ET values than the reference datasets and other products.

ERA5-Land and GLEAM v4.2a exhibit the weakest consistency with the reference datasets, showing low spatial agreement with irrigated areas as well as weaker correspondence in seasonal dynamics compared to the other products. Interestingly, these two datasets also display similar ET patterns across regions.

These findings are consistent with previous studies that have compared global ET datasets across irrigated and agricultural regions. Zhang et al. (2019) reported lower MOD16A2 values compared to PMLv2 over croplands, while Kragh et al. (2023) similarly reported that FLUXCOM RS and PMLv2 show comparable behavior in the Indo-Gangetic Plain. Likewise, Zheng et al. (2022) showed that FLUXCOM, PMLv2, and MOD16 captured irrigation signals in several major irrigated basins (Nile Delta, central Indus Basin, and Heihe River Basin), with FLUXCOM generally producing higher ET values in irrigated zones than PMLv2 and MOD16.

4.1 Factors shaping ET products' performance over irrigated areas

FLUXCOM RS

The FLUXCOM RS machine learning model is trained on data from 224 flux towers, including 27 cropland sites, seven of which are irrigated. Among the nine input features used for ET prediction, six are potentially sensitive to irrigation. One of them is the plant functional type (PFT), which assigns pixels to vegetation classes, such as *cropland*. Because this class was trained on flux tower data from cropland sites—about 25% of which are irrigated (7 out of 27)—irrigation effects may be





implicitly represented in cropland areas. Other key predictors include LST, a variable highly responsive to irrigation and used in four of the input features, as well as vegetation parameters such as EVI and fAPAR, which are included in three.

PMLv2

In PMLv2, the stomatal response to VPD is parameterized separately for each biome, including croplands, using flux tower observations from 95 sites. For the *cropland* biome, the calibration relies on 11 towers, 4 of which are irrigated, meaning that irrigation effects are partially incorporated into the cropland-specific stomatal parameters. These parameters are then applied to all pixels classified as cropland, which may improve the representation of surface resistance, and consequently canopy transpiration, in irrigated areas. PMLv2 also incorporates several MODIS-derived variables that are sensitive to irrigation signals, such as LAI and surface albedo.

SSEBop v6.1

In SSEBop v6.1, ET is computed as the product of a reference evapotranspiration (ET₀) and an evaporative fraction (ETf) derived from LST relative to a dynamically estimated cold/wet reference temperature (T_c). In version 6.1, the T_c benchmark is defined using the FANO algorithm, which identifies cold/wet reference pixels from the local NDVI–LST relationship within a 5 × 5 km moving window. Because both LST and NDVI respond strongly to irrigation, SSEBop v6.1 can capture irrigation signals in spatial patterns and seasonal dynamics. However, SSEBop v6.1 generally produces higher ET values than the other products, which may reflect a positive bias in the Penman–Monteith ET₀ from TerraClimate or a limited reduction of ETf under water-stressed conditions.

MOD16A2

In MOD16A2, ET is estimated using a modified Penman–Monteith equation, where stomatal stress is represented through a surface resistance term (r_s) driven by MODIS-derived vegetation properties (LAI and fAPAR) and meteorological variables, including VPD and air temperature. Unlike FLUXCOM and SSEBop, MOD16A2 does not use LST, and its surface resistance parameters are prescribed for each land-cover class rather than calibrated. The absence of LST information, combined with the static r_s formulation, likely limits the model's sensitivity to irrigation.

325 ERA5-Land

In ERA5-Land, ET is computed using the H-TESSEL land surface model, where soil moisture and VPD are determined by precipitation and atmospheric fields from ERA5. While ERA5 assimilates a wide range of atmospheric observations, neither ERA5 nor ERA5-Land assimilate land-surface observations directly, such as soil moisture or vegetation properties. In our analysis, we do not detect a significant irrigation-related signal being transferred through the atmospheric forcing into ERA5-Land. Because irrigation is not represented, the model typically maintains low soil moisture and high surface resistance (r_s) over irrigated croplands—especially in semi-arid regions—thereby suppressing transpiration. In addition, ERA5-Land uses prescribed, climatological LAI rather than satellite-derived values, which further limits its ability to reflect irrigation-induced vegetation changes.

GLEAM v4.2a



345

350

355

360

365



GLEAM v4.2a estimates soil moisture using a multi-layer water-balance scheme driven by precipitation from MSWEP v2.8, without including any representation of irrigation. Because root-zone soil moisture feeds directly into the evaporative stress factor (Miralles et al., 2025), irrigated croplands are treated as rainfed, leading to excessive vegetation stress during dry periods. GLEAM v4.2a does assimilate surface soil moisture from ESA CCI (Dorigo et al., 2017), but only in the form of anomalies. As these anomalies are computed relative to the satellite product's own climatology, they cannot capture the sustained soil moisture increases induced by irrigation and, therefore, cannot correct the underlying precipitation-driven soil moisture baseline.

Summary of factors explaining ET products' performances over irrigated areas

A key factor influencing how ET products behave over irrigated areas is how they represent vegetation water stress, and particularly which variables drive the formulation of that stress. Products in which surface resistance or stress factors respond to irrigation-sensitive variables—such as LST or vegetation indices—tend to capture irrigation signals more effectively and, therefore, produce higher ET in irrigated regions. In contrast, models in which water stress is strongly influenced by a precipitation-driven soil water balance—such as ERA5-Land and GLEAM v4.2a—tend to underestimate soil moisture in irrigated croplands, leading to excessive modeled stress and consequently lower ET estimates. Another important factor is the inclusion of *in situ* flux tower data from irrigated croplands during model training or calibration. Products such as FLUXCOM RS and PMLv2, which incorporate such sites, tend to show stronger consistency with irrigation-related signals compared to products that do not use such data.

4.2 Considerations on the reference data used for evaluating the ET products

4.2.1 Map of area equipped for irrigation

When assessing the spatial consistency of the ET products using GMIAv5, it is important to recognize that this dataset represents irrigation infrastructure rather than the areas that are actually irrigated at a given time. In reality, the extent of active irrigation varies within and between years depending on water availability, management practices, and policy constraints. This temporal variability is not captured in the dataset and may therefore influence, to some extent, the spatial correlations with ET. The GMIAv5 dataset is also subject to uncertainties in the underlying national statistics, which differ in quality, age, and spatial resolution across countries.

A temporal mismatch also exists between the reference period of GMIAv5 (around 2005) and the time span of the ET products analyzed here. While the map remains broadly representative of irrigation patterns during the 2000–2010 decade, irrigated areas have expanded in several regions since then. Mehta et al. (2024) documented pronounced increases in the area equipped for irrigation in the southern Indus Basin, as well as more moderate growth in the Great Plains, the Mississippi Floodplain, and the Po Valley. Such temporal changes should be considered when interpreting relationships between mean peak-season ET and the mapped irrigation extent. Nevertheless, despite the expansion of irrigated land in some regions since 2005, GMIAv5 still captures the dominant irrigation patterns relevant for the study period.

The relationship between mean peak-season ET and the area equipped for irrigation also depends on how clearly irrigation alters surface variables such as LST and vegetation properties. These signals tend to be more pronounced in semi-arid regions



370

375



(e.g., California Valley, Snake River Plain, Ebro Basin), leading to higher correlations, whereas in more humid areas (e.g., Po Valley, Mississippi Floodplain) they are partly masked by rainfall-driven variability. In addition, in the Indus Basin, the limited spatial variability of the GMIAv5 map—with most pixels showing uniformly high irrigation fractions—further constrains correlation-based analyses.

4.2.2 OpenET

OpenET provides an independent, high-resolution benchmark for evaluating global ET products, combining six modeling approaches that differ substantially in their algorithms and input datasets. However, it remains an ensemble of model simulations rather than direct observations, and therefore inherits the assumptions and limitations of its component models. Volk et al. (2024) found that OpenET tends to underestimate ET over croplands, including irrigated sites, with a mean bias of –5.3 mm month⁻¹ and an average RMSD of about 20 mm month⁻¹ relative to *in situ* flux tower data (metrics computed over the full year, including non-irrigated periods).

Across several regions, Volk et al. (2024) also reported that OpenET often overestimates ET in vineyards and that RMSD values for orchards can reach up to 28 mm month⁻¹. This is particularly relevant for the California Valley, where irrigated agriculture is dominated by perennial crops such as orchards and vineyards. Such crop-specific biases likely contribute to the larger discrepancies observed between OpenET and some global products in this region.

4.2.3 Eddy covariance measurements

Comparisons with eddy covariance data rely on the assumption that irrigation at the instrumented field is broadly representative of conditions within the corresponding 0.1° pixel. This assumption is reasonable in the present study, as both the Livraga and Landriano towers are located in irrigated maize fields surrounded predominantly (though not entirely) by similar irrigated crops. However, variations in irrigation schedules, crop management, or water availability across neighboring fields may still lead to discrepancies between tower-based observations and pixel-averaged ET estimates. In addition, subpixel heterogeneity in land cover, particularly the presence of non-irrigated fields, can further contribute to such differences. While beyond the scope of the present study, future analyses could further explore these site–pixel discrepancies by evaluating ET products at their native spatial resolutions.

5 Conclusions

395

This study presents the first evaluation of six global ET products over irrigated croplands using three independent reference sources: irrigation infrastructure maps, the OpenET ensemble, and eddy-covariance measurements. By assessing spatial patterns, seasonal dynamics, and ET magnitude across diverse agro-climatic regions, we provide a comprehensive comparison of how these products represent irrigation-related ET variability.

The results reveal clear differences among the six datasets. Table 7 summarizes their agreement with the reference datasets, key observations, and factors likely contributing to the observed patterns. FLUXCOM RS, PMLv2, and SSEBop v6.1 show



400

405



the strongest overall consistency, capturing irrigation-related spatial patterns, seasonal dynamics, and ET levels across most regions. FLUXCOM RS and PMLv2 exhibit notably similar behavior, whereas SSEBop v6.1 tends to produce higher ET values. MOD16A2 shows intermediate consistency and generally lower ET estimates. ERA5-Land and GLEAM v4.2a display weaker agreement with the reference datasets. Overall, differences among products primarily reflect (i) how vegetation water stress is represented—whether it responds to irrigation-sensitive variables such as LST and vegetation indices or relies more strongly on precipitation-driven soil-water-balance formulations—and (ii) whether flux tower observations from irrigated croplands were included during model training or calibration.

Table 7. Summary of ET product characteristics over irrigated areas: key observations and factors shaping model responses.

ET product	Agreement with reference data	Key observations	Key factors shaping behavior in irrigated areas
FLUXCOM RS	High	Strong spatial and seasonal consistency; consistent magnitude; similar behavior to PMLv2.	Trained on flux towers including irrigated sites; 6/9 predictors sensitive to irrigation (LST, EVI, fAPAR).
PMLv2	High	Strong spatial and seasonal consistency; consistent magnitude.	Surface resistance calibrated per biome, using flux tower data with irrigated sites; uses MODIS LAI.
SSEBop v6.1	High	Strong spatial consistency; consistent dynamics; high ET values.	Driven mainly by LST and NDVI; uses cold/wet reference pixels to derive the ET fraction.
MOD16A2	Moderate	Captures some spatial and seasonal irrigation signal; low ET values.	Uses MODIS LAI, fAPAR; no biome-specific calibration.
ERA5-Land	Low	Weak spatial and seasonal agreement.	Water stress driven by model soil moisture without explicit irrigation; static LAI; no direct satellite assimilation.
GLEAM v4.2a	Low	Weak spatial and seasonal agreement.	Water stress influenced by precipitation-driven soil moisture and anomaly assimilation; neural-network-based stress mod-
			ule.

These findings point product developers toward clear opportunities for improvement. Strengthening the physical representation of vegetation water stress—particularly by integrating observations that respond directly to irrigation and by calibrating or training models with flux tower data from irrigated croplands—would likely enhance model performance in these environments. For models in which vegetation stress is inferred mainly from precipitation-driven soil-water-balance schemes, incorporating artificial irrigation inputs could improve the reproduction of irrigation-driven ET dynamics, though doing so would require assumptions about the timing and magnitude of water applications. Beyond model development, improved validation efforts are also important. Expanding flux tower networks to better represent the diversity of irrigated systems and climatic conditions would help reduce regional uncertainties and provide stronger constraints for future ET model refinement.

Together, these advances will contribute to more reliable global ET estimates. Such improvements are essential for agricultural water management, drought monitoring, and climate impact assessments, as well as for broader applications such as hydrological modeling, ecosystem monitoring, and water policy design. By identifying the strengths and weaknesses of current global ET products in irrigated landscapes, this study helps users and developers make more informed choices and supports the development of more accurate and resilient tools for global water monitoring and management.





Data availability. The datasets used in this study are available from the following sources: FLUXCOM RS (fluxcom.org); PMLv2 (Google 420 Earth Engine); SSEBop v6.1 (USGS FEWS NET); MOD16A2 (Google Earth Engine); ERA5-Land (Copernicus Climate Data Store); GLEAM4 (gleam.eu); FAO Global Map of Area Equipped for Irrigation (FAO AQUASTAT); WorldCereal global crop maps (ESA World-Cereal); OpenET (openetdata.org). The eddy-covariance measurements used in this study are not publicly available but can be obtained from the data provider upon request.

Author contributions. P.L. designed the study, performed the analysis, and prepared the manuscript. W.D. and C.C. contributed to the study design and interpretation of the results. C.C. provided the flux tower measurements. O.B.-V., Y.Z., S.W., J.M.-S., and G.S. provided the ET datasets and contributed to methodological interpretation. C.A. contributed through critical feedback and manuscript review. All authors contributed to manuscript revision.

Competing interests. The authors declare that they have no competing interests.

Acknowledgements. This work was carried out with support from the European Space Agency under the Climate Change Initiative – Anthropogenic Water Use (CCI-AWU) precursor project (contract number 4000142449/23/I-NB) and the Climate Change Initiative – Land
Evaporation (CCI-E) project (contract number AO/1-12490/24/I-LR). We thank the providers of the MOD16A2, global map of area equipped
for irrigation, OpenET, and flux tower datasets. Any use of trade, firm, or product names is for descriptive purposes only and does not imply
endorsement by the U.S. Government.





References

445

450

455

- Abatzoglou, J. T., Dobrowski, S. Z., Parks, S. A., and Hegewisch, K. C.: TerraClimate, a high-resolution global dataset of monthly climate and climatic water balance from 1958–2015, Scientific Data, 5, 170 191, https://doi.org/10.1038/sdata.2017.191, 2018.
 - Alfieri, L., Avanzi, F., Delogu, F., Gabellani, S., Bruno, G., Campo, L., Libertino, A., Massari, C., Tarpanelli, A., Rains, D., Miralles, D. G., Quast, R., Vreugdenhil, M., Wu, H., and Brocca, L.: High-resolution satellite products improve hydrological modeling in northern Italy, Hydrology and Earth System Sciences, 26, 3921–3939, https://doi.org/10.5194/hess-26-3921-2022, publisher: Copernicus GmbH, 2022.
- 440 Allen, R. G., Tasumi, M., and Trezza, R.: Satellite-Based Energy Balance for Mapping Evapotranspiration with Internalized Calibration (METRIC)—Model, Journal of Irrigation and Drainage Engineering, 133, 380–394, https://doi.org/10.1061/(ASCE)0733-9437(2007)133:4(380), publisher: American Society of Civil Engineers, 2007.
 - Anderson, M. C., Norman, J. M., Kustas, W. P., Houborg, R., Starks, P. J., and Agam, N.: A two-source time-integrated model for estimating surface fluxes using thermal infrared remote sensing, Remote Sensing of Environment, 60, 195–216, https://doi.org/10.1016/S0034-4257(96)00215-5, 1997.
 - Anderson, M. C., Kustas, W. P., and Norman, J. M.: Upscaling Flux Observations from Local to Continental Scales Using Thermal Remote Sensing, Agronomy Journal, 99, 240–254, https://doi.org/10.2134/agronj2005.0096S, 2007.
 - Asmus, C., Hoffmann, P., Pietikäinen, J.-P., Böhner, J., and Rechid, D.: Modeling and evaluating the effects of irrigation on land–atmosphere interaction in southwestern Europe with the regional climate model REMO2020–iMOVE using a newly developed parameterization, Geoscientific Model Development, 16, 7311–7337, https://doi.org/10.5194/gmd-16-7311-2023, publisher: Copernicus GmbH, 2023.
 - Bastiaanssen, W. G. M., Menenti, M., Feddes, R. A., and Holtslag, A. A. M.: A remote sensing surface energy balance algorithm for land (SEBAL): 1. Formulation, Journal of Hydrology, 212–213, 198–212, https://doi.org/10.1016/S0022-1694(98)00253-4, 1998.
 - Beck, H. E., Wood, E. F., Pan, M., Fisher, C. K., Miralles, D. G., van Dijk, A. I. J. M., McVicar, T. R., and Adler, R. F.: MSWEP V2 Global 3-Hourly 0.1° Precipitation: Methodology and Quantitative Assessment, Bulletin of the American Meteorological Society, 100, 473–500, https://doi.org/10.1175/BAMS-D-17-0138.1, 2019.
 - California Department of Water Resources: Report to the Legislature on the 2012–2016 Drought, Tech. rep., California Natural Resources Agency, https://water.ca.gov/-/media/DWR-Website/Web-Pages/Water-Basics/Drought/Files/Publications-And-Reports/CNRA-Drought-Report-final-March-2021.pdf, accessed: 2025-08-08, 2021.
- Chen, L. and Dirmeyer, P. A.: Global observed and modelled impacts of irrigation on surface temperature, International Journal of Climatology, 39, 2587–2600, https://doi.org/10.1002/joc.5973, _eprint: https://rmets.onlinelibrary.wiley.com/doi/pdf/10.1002/joc.5973, 2019.
 - Crow, W. T., Anderson, M. C., Volk, J. M., and Colliander, A.: Value of microwave soil moisture and thermal-infrared evapotranspiration retrievals for the mapping of irrigation coverage, International Journal of Applied Earth Observation and Geoinformation, 143, 104773, https://doi.org/10.1016/j.jag.2025.104773, 2025.
- Dorigo, W., Dietrich, S., Aires, F., Brocca, L., Carter, S., Cretaux, J.-F., Dunkerley, D., Enomoto, H., Forsberg, R., Güntner, A., Hegglin,
 M. I., Hollmann, R., Hurst, D. F., Johannessen, J. A., Kummerow, C., Lee, T., Luojus, K., Looser, U., Miralles, D. G., Pellet, V., Recknagel,
 T., Vargas, C. R., Schneider, U., Schoeneich, P., Schröder, M., Tapper, N., Vuglinsky, V., Wagner, W., Yu, L., Zappa, L., Zemp, M., and
 Aich, V.: Closing the Water Cycle from Observations across Scales: Where Do We Stand?, Bulletin of the American Meteorological
 Society, 102, E1897–E1935, https://doi.org/10.1175/BAMS-D-19-0316.1, publisher: American Meteorological Society Section: Bulletin of the American Meteorological Society, 2021.



490



- 470 Dorigo, W. A., Wagner, W., Albergel, C., Albrecht, F., Balsamo, G., Brocca, L., Chung, D., Ertl, M., Forkel, M., Gruber, A., Haas, E., Hamer, P. D., Hirschi, M., Ikonen, J., de Jeu, R., Kidd, R., Lahoz, W., Liu, Y.-Y., Miralles, D. G., and Lecomte, P.: ESA CCI Soil Moisture for improved Earth system understanding: State-of-the-art and future directions, Remote Sensing of Environment, 203, 185–215, https://doi.org/10.1016/j.rse.2017.07.001, 2017.
- Entekhabi, D., Njoku, E. G., O'Neill, P. E., Kellogg, K. H., Crow, W. T., Edelstein, W. N., Entin, J. K., Goodman, S. D., Jackson, T. J., Johnson, J., et al.: The Soil Moisture Active Passive (SMAP) Mission, Proceedings of the IEEE, 98, 704–716, https://doi.org/10.1109/JPROC.2010.2043918, 2010.
 - Etchanchu, J., Demarty, J., Dezetter, A., Farhani, N., Thiam, P. B., Allies, A., Bodian, A., Boulet, G., Chahinian, N., Diop, L., Mainassara, I., Ndiaye, P. M., Ollivier, C., Olioso, A., and Roupsard, O.: Multiscale analysis of existing actual evapotranspiration products over agropastoral Sahel, Journal of Hydrology, 651, 132 585, https://doi.org/10.1016/j.jhydrol.2024.132585, 2025.
- 480 FAO: WaPOR, FAO's portal to monitor water productivity through open access of remotely sensed derived data, Rome: Food and Agriculture Organization of the United Nations, http://www.fao.org/land-water/databases-and-software/wapor/en/, 2018.
 - Fisher, J. B., Tu, K. P., and Baldocchi, D. D.: Evapotranspiration models based on the Penman–Monteith equation and energy balance, Remote Sensing of Environment, 112, 901–919, https://doi.org/10.1016/j.rse.2007.06.025, 2008.
- Fisher, J. B., Melton, F., Middleton, E., Hain, C., Anderson, M., Allen, R., McCabe, M. F., Hook, S., Baldocchi, D., Townsend, P. A., Kilic, A., Tu, K., Miralles, D. G., Perret, J., Lagouarde, J.-P., Waliser, D., Purdy, A. J., French, A., Schimel, D., Famiglietti, J., Stephens, G., and Wood, E. F.: The future of evapotranspiration: Global requirements for ecosystem functioning, carbon and climate feedbacks, agricultural management, and water resources, Water Resources Research, 53, 2618–2626, https://doi.org/10.1002/2016WR020175, 2017.
 - Gelaro, R., McCarty, W., Suárez, M. J., Todling, R., Molod, A., Takacs, L., Randles, C. A., Darmenov, A., Bosilovich, M. G., Reichle, R., Wargan, K., Coy, L., Cullather, R., Draper, C., Akella, S., Buchard, V., Conaty, A., Silva, A. M. d., Gu, W., Kim, G.-K., Koster, R., Lucchesi, R., Merkova, D., Nielsen, J. E., Partyka, G., Pawson, S., Putman, W., Rienecker, M., Schubert, S. D., Sienkiewicz, M., and Zhao, B.: The Modern-Era Retrospective Analysis for Research and Applications, Version 2 (MERRA-2), Journal of Climate, 30, 5419–5454,
 - Hobeichi, S., Abramowitz, G., Evans, J., and Ukkola, A.: Derived Optimal Linear Combination Evapotranspiration (DOLCE): a global gridded synthesis ET estimate, Hydrology and Earth System Sciences, 22, 1317–1336, https://doi.org/10.5194/hess-22-1317-2018, 2018.
- Hong, S., Deng, H., Zheng, Z., Deng, Y., Chen, X., Gao, L., Chen, Y., and Liu, M.: The influence of variations in actual evapotranspiration on drought in China's Southeast River basin, Scientific Reports, 13, 21 336, https://doi.org/10.1038/s41598-023-48663-8, publisher: Nature Publishing Group, 2023.

https://doi.org/10.1175/JCLI-D-16-0758.1, publisher: American Meteorological Society Section: Journal of Climate, 2017.

- Hulley, G. C., Malakar, N. K., Islam, T., and Freepartner, R. J.: NASA's MODIS and VIIRS Land Surface Temperature and Emissivity
 Products: A Long-Term and Consistent Earth System Data Record, IEEE Journal of Selected Topics in Applied Earth Observations and
 Remote Sensing, 11, 522–535, https://doi.org/10.1109/JSTARS.2017.2779330, 2018.
 - Hulsman, P., Keune, J., Koppa, A., Schellekens, J., and Miralles, D. G.: Incorporating plant access to groundwater in existing global, satellite-based evaporation estimates, Water Resources Research, 59, https://doi.org/10.1029/2022WR033731, 2023.
- Jung, M., Koirala, S., Weber, U., Ichii, K., Gans, F., Camps-Valls, G., Papale, D., Schwalm, C., Tramontana, G., and Reichstein, M.: The FLUXCOM ensemble of global land-atmosphere energy fluxes, Scientific Data, 6, 74, https://doi.org/10.1038/s41597-019-0076-8, publisher: Nature Publishing Group, 2019.



520

540



- Knipper, K. R., Kustas, W. P., Anderson, M. C., Alsina, M. M., Hain, C. R., Alfieri, J. G., Prueger, J. H., Gao, F., McKee, L. G., and Sanchez, L. A.: Using high-spatiotemporal thermal satellite ET retrievals for operational water use and stress monitoring in a California vineyard, Remote Sensing, 11, 2124, https://doi.org/10.3390/rs11182124, 2019.
- Koppa, A., Rains, D., Hulsman, P., Poyatos, R., and Miralles, D. G.: A deep learning-based hybrid model of global terrestrial evaporation,

 Nature Communications, 13, 1912, https://doi.org/10.1038/s41467-022-29543-7, 2022.
 - Kragh, S. J., Fensholt, R., Stisen, S., and Koch, J.: The precision of satellite-based net irrigation quantification in the Indus and Ganges basins, Hydrology and Earth System Sciences, 27, 2463–2478, https://doi.org/10.5194/hess-27-2463-2023, publisher: Copernicus GmbH, 2023.
- Lehmann, F., Vishwakarma, B. D., and Bamber, J.: How well are we able to close the water budget at the global scale?, Hydrology and Earth System Sciences, 26, 35–54, https://doi.org/10.5194/hess-26-35-2022, publisher: Copernicus GmbH, 2022.
 - Liu, W., Wang, L., Zhou, J., Li, Y., Sun, F., Fu, G., Li, X., and Sang, Y.-F.: A worldwide evaluation of basin-scale evapotranspiration estimates against the water balance method, Journal of Hydrology, 538, 82–95, https://doi.org/10.1016/j.jhydrol.2016.04.006, 2016.
 - Liu, X., Yang, K., Ferreira, V. G., and Bai, P.: Hydrologic Model Calibration With Remote Sensing Data Products in Global Large Basins, Water Resources Research, 58, e2022WR032929, https://doi.org/10.1029/2022WR032929, _eprint: https://agupubs.onlinelibrary.wiley.com/doi/pdf/10.1029/2022WR032929, 2022.
 - Lunel, T., Boone, A. A., and Le Moigne, P.: Irrigation strongly influences near-surface conditions and induces breeze circulation: Observational and model-based evidence, Quarterly Journal of the Royal Meteorological Society, 150, 2798–2819, https://doi.org/10.1002/qj.4736, _eprint: https://rmets.onlinelibrary.wiley.com/doi/pdf/10.1002/qj.4736, 2024.
- Masseroni, D., Ercolani, G., Corbari, C., and Mancini, M.: Accuracy of turbulent flux measurements through the use of high frequency data by eddy covariance tower: the case study of Landriano (PV), Italy, https://air.unimi.it/handle/2434/231850, accepted: 2014-02-27T15:08:14Z Publisher: AIAM, 2013.
 - McCabe, M. F., Ershadi, A., Jimenez, C., Miralles, D. G., Michel, D., and Wood, E. F.: The GEWEX LandFlux project: evaluation of model evaporation using tower-based and globally gridded forcing data, Geoscientific Model Development, 9, 283–305, https://doi.org/10.5194/gmd-9-283-2016, publisher: Copernicus GmbH, 2016.
- McDermid, S., Nocco, M., Lawston-Parker, P., Keune, J., Pokhrel, Y., Jain, M., Jägermeyr, J., Brocca, L., Massari, C., Jones, A. D., Vahmani, P., Thiery, W., Yao, Y., Bell, A., Chen, L., Dorigo, W., Hanasaki, N., Jasechko, S., Lo, M.-H., Mahmood, R., Mishra, V., Mueller, N. D., Niyogi, D., Rabin, S. S., Sloat, L., Wada, Y., Zappa, L., Chen, F., Cook, B. I., Kim, H., Lombardozzi, D., Polcher, J., Ryu, D., Santanello, J., Satoh, Y., Seneviratne, S., Singh, D., and Yokohata, T.: Irrigation in the Earth system, Nature Reviews Earth & Environment, 4, 435–453, https://doi.org/10.1038/s43017-023-00438-5, publisher: Nature Publishing Group, 2023.
- McDermid, S. S., Montes, C., Cook, B. I., Puma, M. J., Kiang, N. Y., and Aleinov, I.: The Sensitivity of Land–Atmosphere Coupling to Modern Agriculture in the Northern Midlatitudes, Journal of Climate, 32, 465–484, https://doi.org/10.1175/JCLI-D-17-0799.1, publisher: American Meteorological Society Section: Journal of Climate, 2019.
 - McNamara, I., Baez-Villanueva, O. M., Zomorodian, A., Ayyad, S., Zambrano-Bigiarini, M., Zaroug, M., Mersha, A., Nauditt, A., Mbuliro, M., Wamala, S., and Ribbe, L.: How well do gridded precipitation and actual evapotranspiration products represent the key water balance components in the Nile Basin?, Journal of Hydrology: Regional Studies, 37, 100 884, https://doi.org/10.1016/j.ejrh.2021.100884, 2021.
 - Mehta, P., Siebert, S., Kummu, M., Deng, Q., Ali, T., Marston, L., Xie, W., and Davis, K. F.: Half of twenty-first century global irrigation expansion has been in water-stressed regions, Nature Water, 2, 254–261, https://doi.org/10.1038/s44221-024-00206-9, 2024.





- Melton, F. S., Johnson, L. F., Lund, C. P., Pierce, L. L., Michaelis, A. R., Hiatt, S. H., Guzman, A., Adhikari, D. D., Purdy, A. J., Rosevelt,
 C., Votava, P., Trout, T. J., Temesgen, B., Frame, K., Sheffner, E. J., and Nemani, R. R.: Satellite Irrigation Management Support With the
 Terrestrial Observation and Prediction System: A Framework for Integration of Satellite and Surface Observations to Support Improvements in Agricultural Water Resource Management, IEEE Journal of Selected Topics in Applied Earth Observations and Remote Sensing,
 5, 1709–1721, https://doi.org/10.1109/JSTARS.2012.2214474, 2012.
- Melton, F. S., Huntington, J., Grimm, R., Herring, J., Hall, M., Rollison, D., Erickson, T., Allen, R., Anderson, M., Fisher, J. B., Kilic, A., Senay, G. B., Volk, J., Hain, C., Johnson, L., Ruhoff, A., Blankenau, P., Bromley, M., Carrara, W., Daudert, B., Doherty, C., Dunkerly, C., Friedrichs, M., Guzman, A., Halverson, G., Hansen, J., Harding, J., Kang, Y., Ketchum, D., Minor, B., Morton, C., Ortega-Salazar, S., Ott, T., Ozdogan, M., ReVelle, P. M., Schull, M., Wang, C., Yang, Y., and Anderson, R. G.: OpenET: Filling a Critical Data Gap in Water Management for the Western United States, JAWRA Journal of the American Water Resources Association, 58, 971–994, https://doi.org/10.1111/1752-1688.12956, eprint: https://onlinelibrary.wiley.com/doi/pdf/10.1111/1752-1688.12956, 2022.
- Miralles, D. G., Bonte, O., Koppa, A., Baez-Villanueva, O. M., Tronquo, E., Zhong, F., Beck, H. E., Hulsman, P., Dorigo, W., Verhoest,

 N. E. C., and Haghdoost, S.: GLEAM4: global land evaporation and soil moisture dataset at 0.1° resolution from 1980 to near present,

 Scientific Data, 12, 416, https://doi.org/10.1038/s41597-025-04610-y, publisher: Nature Publishing Group, 2025.
 - Mu, Q., Zhao, M., and Running, S. W.: Improvements to a MODIS global terrestrial evapotranspiration algorithm, Remote Sensing of Environment, 115, 1781–1800, https://doi.org/10.1016/j.rse.2011.02.019, 2011.
- Mueller, B., Hirschi, M., Jimenez, C., Ciais, P., Dirmeyer, P. A., Dolman, A. J., Fisher, J. B., Jung, M., Ludwig, F., Maignan, F., Miralles, D. G., McCabe, M. F., Reichstein, M., Sheffield, J., Wang, K., Wood, E. F., Zhang, Y., and Seneviratne, S. I.: Benchmark products for land evapotranspiration: LandFlux-EVAL multi-data set synthesis, Hydrology and Earth System Sciences, 17, 3707–3720, https://doi.org/10.5194/hess-17-3707-2013, publisher: Copernicus GmbH, 2013.
- Muñoz-Sabater, J., Dutra, E., Agustí-Panareda, A., Albergel, C., Arduini, G., Balsamo, G., Boussetta, S., Choulga, M., Harrigan, S., Hersbach, H., Martens, B., Miralles, D. G., Piles, M., Rodríguez-Fernández, N. J., Zsoter, E., Buontempo, C., and Thépaut, J.-N.: ERA5-Land:
 a state-of-the-art global reanalysis dataset for land applications, Earth System Science Data, 13, 4349–4383, https://doi.org/10.5194/essd-13-4349-2021, publisher: Copernicus GmbH, 2021.
 - Nana, E., Corbari, C., and Bocchiola, D.: A model for crop yield and water footprint assessment: Study of maize in the Po valley, Agricultural Systems, 127, 139–149, https://doi.org/10.1016/j.agsy.2014.03.006, 2014.
- Nelson, J. A., Walther, S., Gans, F., Kraft, B., Weber, U., Novick, K., Buchmann, N., Migliavacca, M., Wohlfahrt, G., Šigut, L., Ibrom, A.,
 Papale, D., Göckede, M., Duveiller, G., Knohl, A., Hörtnagl, L., Scott, R. L., Dušek, J., Zhang, W., Hamdi, Z. M., Reichstein, M., Aranda-Barranco, S., Ardö, J., Op de Beeck, M., Billesbach, D., Bowling, D., Bracho, R., Brümmer, C., Camps-Valls, G., Chen, S., Cleverly, J. R., Desai, A., Dong, G., El-Madany, T. S., Euskirchen, E. S., Feigenwinter, I., Galvagno, M., Gerosa, G. A., Gielen, B., Goded, I., Goslee, S., Gough, C. M., Heinesch, B., Ichii, K., Jackowicz-Korczynski, M. A., Klosterhalfen, A., Knox, S., Kobayashi, H., Kohonen, K.-M., Korkiakoski, M., Mammarella, I., Gharun, M., Marzuoli, R., Matamala, R., Metzger, S., Montagnani, L., Nicolini, G., O'Halloran, T.,
- Ourcival, J.-M., Peichl, M., Pendall, E., Ruiz Reverter, B., Roland, M., Sabbatini, S., Sachs, T., Schmidt, M., Schwalm, C. R., Shekhar, A., Silberstein, R., Silveira, M. L., Spano, D., Tagesson, T., Tramontana, G., Trotta, C., Turco, F., Vesala, T., Vincke, C., Vitale, D., Vivoni, E. R., Wang, Y., Woodgate, W., Yepez, E. A., Zhang, J., Zona, D., and Jung, M.: X-BASE: the first terrestrial carbon and water flux products from an extended data-driven scaling framework, FLUXCOM-X, Biogeosciences, 21, 5079–5115, https://doi.org/10.5194/bg-21-5079-2024, publisher: Copernicus GmbH, 2024.



595



- 580 Oki, T. and Kanae, S.: Global Hydrological Cycles and World Water Resources, Science, 313, 1068–1072, https://doi.org/10.1126/science.1128845, publisher: American Association for the Advancement of Science, 2006.
 - Pascolini-Campbell, M. A., Reager, J. T., and Fisher, J. B.: GRACE-based Mass Conservation as a Validation Target for Basin-Scale Evapotranspiration in the Contiguous United States, Water Resources Research, 56, e2019WR026594, https://doi.org/10.1029/2019WR026594, eprint: https://agupubs.onlinelibrary.wiley.com/doi/pdf/10.1029/2019WR026594, 2020.
- Rodell, M., Houser, P. R., Jambor, U., Gottschalck, J., Mitchell, K., Meng, C.-J., Arsenault, K., Cosgrove, B., Radakovich, J., Bosilovich, M., Entin, J. K., Walker, J. P., Lohmann, D., and Toll, D.: The Global Land Data Assimilation System, Bulletin of the American Meteorological Society, 85, 381–394, https://doi.org/10.1175/BAMS-85-3-381, publisher: American Meteorological Society Section: Bulletin of the American Meteorological Society, 2004.
- Senay, G.: Satellite Psychrometric Formulation of the Operational Simplified Surface Energy Balance (SSEBop) Model for Quantifying and Mapping Evapotranspiration, Applied Engineering in Agriculture, 34, 555–566, https://doi.org/10.13031/aea.12614, 2018.
 - Senay, G. B., Budde, M. E., Verdin, J. P., and Melesse, A. M.: Operational evapotranspiration mapping using remote sensing and weather datasets: A new parameterization for the SSEB approach, Journal of the American Water Resources Association, 49, 577–591, https://doi.org/10.1111/jawr.12057, 2013.
 - Senay, G. B., Friedrichs, M., Singh, R. K., and Velpuri, N. M.: Evaluating Landsat 8 evapotranspiration for water use mapping in the Colorado River Basin, Remote Sensing of Environment, 185, 171–185, https://doi.org/10.1016/j.rse.2015.12.043, 2016.
 - Senay, G. B., Parrish, G. E. L., Schauer, M., Friedrichs, M., Khand, K., Boiko, O., Kagone, S., Dittmeier, R., Arab, S., and Ji, L.: Improving the Operational Simplified Surface Energy Balance Evapotranspiration Model Using the Forcing and Normalizing Operation, Remote Sensing, 15, 260, https://doi.org/10.3390/rs15010260, publisher: Multidisciplinary Digital Publishing Institute, 2023.
- Seneviratne, S. I., Corti, T., Davin, E. L., Hirschi, M., Jaeger, E. B., Lehner, I., Orlowsky, B., and Teuling, A. J.: Investigating soil moisture–climate interactions in a changing climate: A review, Earth-Science Reviews, 99, 125–161, https://doi.org/10.1016/j.earscirev.2010.02.004, 2010.
 - Siebert, S., Henrich, V., Frenken, K., and Burke, J.: Update of the digital global map of irrigation areas to version 5., https://doi.org/10.13140/2.1.2660.6728, 2013.
- Sriwongsitanon, N., Suwawong, T., Thianpopirug, S., Williams, J., Jia, L., and Bastiaanssen, W.: Validation of seven global remotely sensed ET products across Thailand using water balance measurements and land use classifications, Journal of Hydrology: Regional Studies, 30, 100 709, https://doi.org/10.1016/j.ejrh.2020.100709, 2020.
 - Thiery, W., Davin, E. L., Lawrence, D. M., Hirsch, A. L., Hauser, M., and Seneviratne, S. I.: Present-day irrigation mitigates heat extremes, Journal of Geophysical Research: Atmospheres, 122, 1403–1422, https://doi.org/10.1002/2016JD025740, _eprint: https://agupubs.onlinelibrary.wiley.com/doi/pdf/10.1002/2016JD025740, 2017.
- Thiery, W., Visser, A. J., Fischer, E. M., Hauser, M., Hirsch, A. L., Lawrence, D. M., Lejeune, Q., Davin, E. L., and Seneviratne, S. I.: Warming of hot extremes alleviated by expanding irrigation, Nature Communications, 11, 290, https://doi.org/10.1038/s41467-019-14075-4, 2020.
 - Valentini, R., Arneth, A., Bombelli, A., Castaldi, S., Gatti, R. C., Chevallier, F., Ciais, P., Grieco, E., Hartmann, J., Henry, M., Houghton, R. A., Jung, M., Kutsch, W. K., Malhi, Y., Mayorga, E., Merbold, L., Murray-Tortarolo, G., Papale, D., Peylin, P., Poulter, B., Raymond,
- P. A., Santini, M., Sitch, S., Laurin, G. V., van der Werf, G. R., Williams, C. A., and Scholes, R. J.: A full greenhouse gases budget of Africa: synthesis, uncertainties, and vulnerabilities, Biogeosciences, 11, 381–407, https://doi.org/10.5194/bg-11-381-2014, 2014.



635



- van Dijk, A. I. J. M. and Bruijnzeel, L. A.: Modelling rainfall interception by vegetation of variable density using an adapted analytical model. Part 1. Model description, Journal of Hydrology, 247, 230–238, https://doi.org/10.1016/s0022-1694(01)00392-4, 2001.
- Van Tricht, K., Degerickx, J., Gilliams, S., Zanaga, D., Battude, M., Grosu, A., Brombacher, J., Lesiv, M., Laso Bayas, J. C., Karanam,
 S., Fritz, S., Becker-Reshef, I., Franch, B., Mollá-Bononad, B., Boogaard, H., Pratihast, A. K., Koetz, B., Szantoi, Z., and Defourny,
 P.: WorldCereal: a dynamic open-source system for global-scale, seasonal, and reproducible crop and irrigation mapping, Earth System
 Science Data, 15, 5491–5515, https://doi.org/10.5194/essd-15-5491-2023, 2023.
 - Volk, J. M., Huntington, J. L., Melton, F. S., Allen, R., Anderson, M., Fisher, J. B., Kilic, A., Ruhoff, A., Senay, G. B., Minor, B., Morton, C., Ott, T., Johnson, L., Comini de Andrade, B., Carrara, W., Doherty, C. T., Dunkerly, C., Friedrichs, M., Guzman, A., Hain, C., Halverson,
- G., Kang, Y., Knipper, K., Laipelt, L., Ortega-Salazar, S., Pearson, C., Parrish, G. E. L., Purdy, A., ReVelle, P., Wang, T., and Yang, Y.: Assessing the accuracy of OpenET satellite-based evapotranspiration data to support water resource and land management applications, Nature Water, 2, 193–205, https://doi.org/10.1038/s44221-023-00181-7, publisher: Nature Publishing Group, 2024.
 - Wang, Z., Zhan, C., Ning, L., and Guo, H.: Evaluation of global terrestrial evapotranspiration in CMIP6 models, Theoretical and Applied Climatology, 143, 521–531, https://doi.org/10.1007/s00704-020-03437-4, 2021.
- Weerasinghe, I., Bastiaanssen, W., Mul, M., Jia, L., and van Griensven, A.: Can we trust remote sensing evapotranspiration products over Africa?, Hydrology and Earth System Sciences, 24, 1565–1586, https://doi.org/10.5194/hess-24-1565-2020, publisher: Copernicus GmbH, 2020.
 - Zhang, C. and Long, D.: Estimating Spatially Explicit Irrigation Water Use Based on Remotely Sensed Evapotranspiration and Modeled Root Zone Soil Moisture, Water Resources Research, 57, e2021WR031382, https://doi.org/10.1029/2021WR031382, _eprint: https://agupubs.onlinelibrary.wiley.com/doi/pdf/10.1029/2021WR031382, 2021.
 - Zhang, Y., Kong, D., Gan, R., Chiew, F. H. S., McVicar, T. R., Zhang, Q., and Yang, Y.: Coupled estimation of 500m and 8-day resolution global evapotranspiration and gross primary production in 2002–2017, Remote Sensing of Environment, 222, 165–182, https://doi.org/10.1016/j.rse.2018.12.031, 2019.
- Zheng, C., Jia, L., and Hu, G.: Global land surface evapotranspiration monitoring by ETMonitor model driven by multi-source satellite earth observations, Journal of Hydrology, 613, 128 444, https://doi.org/10.1016/j.jhydrol.2022.128444, 2022.
 - Zhong, F., Jiang, S., Dijk, A. I. J. M. v., Ren, L., Schellekens, J., and Miralles, D. G.: Revisiting large-scale interception patterns constrained by a synthesis of global experimental data, Hydrology and Earth System Sciences, 26, 5647–5667, https://doi.org/10.5194/hess-26-5647-2022, 2022.
- Zipper, S., Kastens, J., Foster, T., Wilson, B. B., Melton, F., Grinstead, A., Deines, J. M., Butler, J. J., and Marston, L. T.: Estimating irrigation water use from remotely sensed evapotranspiration data: Accuracy and uncertainties at field, water right, and regional scales, Agricultural Water Management, 303, 109 036, https://doi.org/10.1016/j.agwat.2024.109036, 2024.